


Article

Modeling Analysis of Nocturnal Nitrate Formation Pathways during Co-Occurrence of Ozone and PM_{2.5} Pollution in North China Plain

Wei Dai ^{1,*}, Keqiang Cheng ¹, Xiangpeng Huang ² and Mingjie Xie ¹ 

¹ Collaborative Innovation Center of Atmospheric Environment and Equipment Technology, Jiangsu Key Laboratory of Atmospheric Environment Monitoring and Pollution Control, School of Environmental Science and Engineering, Nanjing University of Information Science & Technology, Nanjing 210044, China

² Shanghai Key Laboratory of Atmospheric Particle Pollution and Prevention, Department of Environmental Science and Engineering, Fudan University, Shanghai 200438, China; huangxp@fudan.edu.cn

* Correspondence: daiweideemail@nuist.edu.cn

Abstract: The rapid formation of secondary nitrate (NO₃⁻) contributes significantly to the nocturnal increase of PM_{2.5} and has been shown to be a critical factor for aerosol pollution in the North China Plain (NCP) region in summer. To explore the nocturnal NO₃⁻ formation pathways and the influence of ozone (O₃) on NO₃⁻ production, the WRF-CMAQ model was utilized to simulate O₃ and PM_{2.5} co-pollution events in the NCP region. The simulation results demonstrated that heterogeneous hydrolysis of dinitrogen pentoxide (N₂O₅) accounts for 60% to 67% of NO₃⁻ production at night (22:00 to 05:00) and is the main source of nocturnal NO₃⁻. O₃ enhances the formation of NO₃ radicals, thereby further promoting nocturnal N₂O₅ production. In the evening (20:00 to 21:00), O₃ sustains the formation of hydroxyl (OH) radicals, resulting in the reaction between OH radicals and nitrogen dioxide (NO₂), which accounts for 48% to 64% of NO₃⁻ formation. Our results suggest that effective control of O₃ pollution in NCP can also reduce NO₃⁻ formation at night.

Keywords: nocturnal PM_{2.5} pollution; nitrate aerosol; nitric acid; WRF-CMAQ



Citation: Dai, W.; Cheng, K.; Huang, X.; Xie, M. Modeling Analysis of Nocturnal Nitrate Formation Pathways during Co-Occurrence of Ozone and PM_{2.5} Pollution in North China Plain. *Atmosphere* **2024**, *15*, 1220. <https://doi.org/10.3390/atmos15101220>

Academic Editors: Kei Sato and Daniele Contini

Received: 15 August 2024

Revised: 10 September 2024

Accepted: 12 October 2024

Published: 13 October 2024



Copyright: © 2024 by the authors. Licensee MDPI, Basel, Switzerland. This article is an open access article distributed under the terms and conditions of the Creative Commons Attribution (CC BY) license (<https://creativecommons.org/licenses/by/4.0/>).

1. Introduction

Fine particulate matter (PM_{2.5}) in the air influences human health and causes climate change by altering the radiation balance [1,2]. The components of PM_{2.5} include nitrate (NO₃⁻), ammonium (NH₄⁺), sulfate (SO₄²⁻), and organic aerosols (OA), which originate from both primary emissions (e.g., anthropogenic activities, wildfires, and dust) and secondary formation. Due to the implemented emission reduction policies, the concentration of PM_{2.5} in eastern China has decreased significantly [3]. However, compared with other secondary components of PM_{2.5}, the concentration of NO₃⁻ declined more slowly [4–6]. Previous studies have indicated that NO₃⁻ is gradually becoming a crucial component of PM_{2.5}, especially during severe haze events in the North China Plain (NCP) region [7–9].

The NO₃⁻ is formed by the gas-to-particle partitioning of nitric acid (HNO₃), a process that depends on temperature, relative humidity, and ammonia (NH₃) [10–12]. As an essential precursor of NO₃⁻, the formation processes of HNO₃ are complicated. Previous studies have shown that there are three main pathways for the formation of HNO₃: (1) the oxidation reaction of hydroxyl (OH) radicals and nitrogen dioxide (NO₂), (2) the heterogeneous hydrolysis reaction of dinitrogen pentoxide (N₂O₅) at the aerosol surface under the condition of high relative humidity and (3) serial reactions of nitrate (NO₃) radicals with oxygenated volatile organic compounds (OVOCs) [13–16]. Previous studies have suggested that the reaction of OH radicals and NO₂ (OH + NO₂) dominates the production of HNO₃ during the daytime and accounts for more than 90% of the total production [13,17,18]. During the night, the heterogeneous hydrolysis of N₂O₅ (HET N₂O₅)

becomes the main production process of HNO_3 , accounting for 44% to 97%, replacing the “OH + NO_2 ” pathway [19–21]. This is because the OH and NO_3 radicals dominate the atmospheric oxidation capacity during the day and night, respectively, and drive the chemical reactions in the troposphere. The production of the OH radical depends on photolysis. However, the NO_3 radical is mainly formed by the reaction of NO_2 with ozone (O_3) and removed by photolysis and reaction with NO during the daytime [22–26].

Since 2013, the Chinese government has implemented strict emission reduction policies in order to improve air quality. As a result, the concentration of $\text{PM}_{2.5}$ has continued to decline in recent years, while the O_3 concentration has reversed. O_3 is not only harmful to human health and plants but is also an important oxidant in the troposphere [27]. From 2013 to 2019, the mean daily maximum 8-h average (MDA8) of O_3 in summer in the NCP region illustrated an increasing trend of 3.3 ppb per year [3,28]. The emission reduction policies were unable to completely prevent the occurrence of $\text{PM}_{2.5}$ pollution, owing to complex meteorological conditions and the formation of secondary $\text{PM}_{2.5}$ [29–31]. Observation and simulation studies have suggested that the nocturnal formation of NO_3^- dominates the chemical process of $\text{PM}_{2.5}$, accounting for about 30% of its composition during haze events [19,32,33]. In addition, previous studies have shown that high concentrations of O_3 enhanced atmospheric oxidation capacity, accelerating the generation of other secondary pollutants during the warm season [34–36]. Wang et al. have indicated that with the increase of MDA8 O_3 during summer (June–July) in NCP, there is a corresponding rise in the proportion of NO_3^- [37].

During the summer, the process of NO_3^- formation induced by O_3 is more complex, and there is comparatively less research on this topic. Previous research has predominantly focused on individual $\text{PM}_{2.5}$ pollution events during the cold season. Although the average $\text{PM}_{2.5}$ concentration is lower in summer than in winter, there is still insufficient research on the mechanisms that lead to the rapid increase of NO_3^- during summer nights. In this study, we investigated the nocturnal formation processes of NO_3^- during combined pollution events with O_3 and $\text{PM}_{2.5}$ in the NCP region. The WRF-CMAQ model was used to simulate the O_3 - $\text{PM}_{2.5}$ combined pollution process in summer in the North China Plain (NCP) region, and the process analysis (PA) tool was used to diagnose the series reactions rate for the formation of HNO_3 , N_2O_5 and NO_3 radicals. The purpose of this study is to quantify the chemical pathways of NO_3^- formation during O_3 and $\text{PM}_{2.5}$ co-pollution events and to investigate the effects of O_3 on NO_3^- formation.

2. Methods

2.1. Model Configuration

The Community Multiscale Air Quality (CMAQ, version 5.3.3) model was applied to investigate the formation of nocturnal NO_3^- during O_3 and $\text{PM}_{2.5}$ co-pollution episodes in the NCP region [38]. We configure the CMAQ model with two nested domains, as depicted in Figure 1. The parent domain (D01) covers most of eastern China with a horizontal resolution of 27 km. The nested domain (D02) focuses on the NCP region (marked by the blue dashed square in Figure 1) with a horizontal resolution of 9 km. The CMAQ model utilized the State-wide Air Pollution Research Center Version 07 (SAPRC07tic) photochemical mechanism and the seventh-generation aerosol (AERO7i) module [39]. The Weather Research and Forecasting (WRF) version 4.2.3 provided essential meteorological field for the CMAQ model, with initial and boundary conditions from the European Center for Medium-Range Weather Forecasts (ECMWF) producing ERA5 reanalysis data, which has a spatial resolution of $0.25^\circ \times 0.25^\circ$ [40]. The detailed information and physical configurations of the WRF model are consistent with Chen et al. [41]. Anthropogenic emissions were obtained from the Multi-resolution Emission Inventory for China (MEIC, version 1.4) and the MIX for surrounding areas (<http://meicmodel.org/>, last access: 20 June 2024), which was developed by Tsinghua University [42]. The biogenic emissions were generated by using the Model of Emissions of Gas and Aerosols from Nature (MEGAN, Version 2.1,

Guenther, Karl [43]). The real-time biomass burning emissions were calculated from the Global Fire Emission Database Version 4 (GFED4), including small fires (GFED4s) [44].

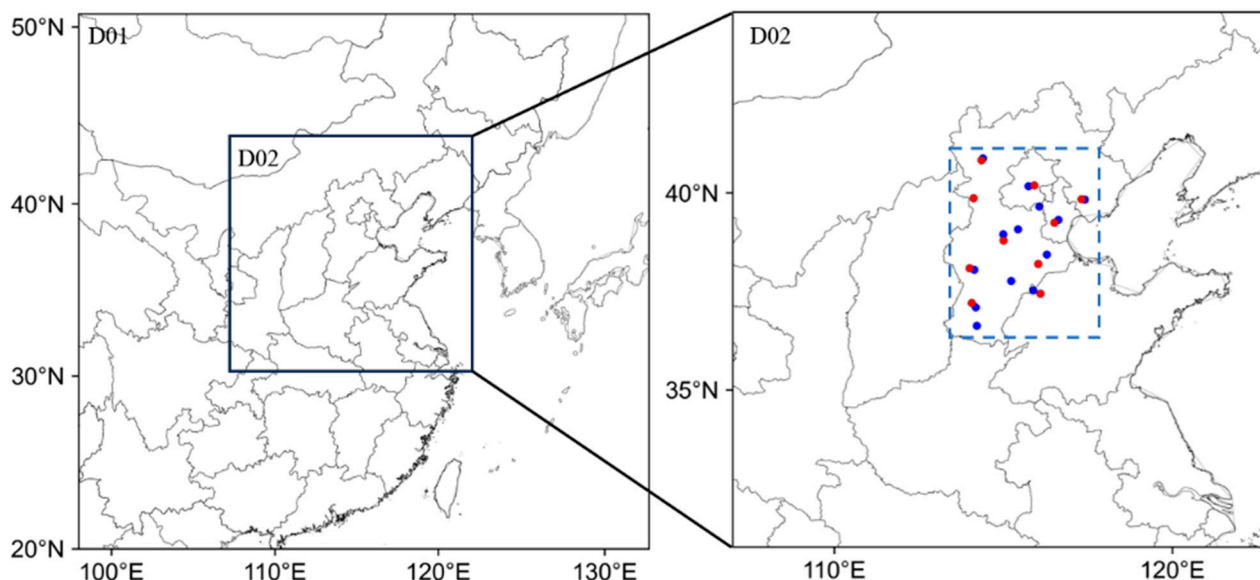


Figure 1. The WRF-CMAQ simulation domains, with red and blue dots, denote the locations of meteorological and environmental observation sites. The blue dashed rectangle marked North China Plain.

The process analysis (PA) tool in the CMAQ model was used to diagnose the integrated process rate (IPR) and integrated reaction rate (IRR) for each species [45]. In this study, the IRR analysis tool was employed to explore the complicated gas-phase chemical reaction pathways of the HNO_3 and N_2O_5 [32,46,47]. The details of HNO_3 , N_2O_5 , and NO_3 radical chemical production pathways are listed in Table 1. In order to analyze easily, these chemical reaction pathways are grouped into “OH + NO_2 ”, “HET N_2O_5 ”, “ NO_3 + VOC”, “Others”, “ NO_2 + NO_3 ” and “ O_3 + NO_2 ”, according to their contributions [46,48].

Table 1. Reactions of HNO_3 and N_2O_5 involved in CMAQ v5.3.3 (SAPRC07tic).

ID	Name	Pathway	Descriptions
1	OH_NO ₂	OH + NO ₂	OH + NO ₂ → HNO ₃
2	N ₂ O ₅ _H ₂ O	HET N ₂ O ₅	N ₂ O ₅ + H ₂ O → 2 × HNO ₃
3	HET_N ₂ O ₅	HET N ₂ O ₅	N ₂ O ₅ → HNO ₃
4	NO ₃ _VOC	NO ₃ + VOC	VOCs + NO ₃ → HNO ₃
5	HET_NO ₂	Others	NO ₂ → 0.5 × HNO ₃
6	HET_NO ₃	Others	NO ₃ → HNO ₃
7	FromHydro	Others	AMTNO3J → HNO ₃ ; AISOPNNJ → 2.0 × HNO ₃
8	NO ₃ _HO ₂	Others	NO ₃ + HO ₂ → 0.2 × HNO ₃
9	NO ₂ _NO ₃	NO ₂ + NO ₃	NO ₂ + NO ₃ → N ₂ O ₅
10	O ₃ _NO ₂	O ₃ + NO ₂	O ₃ + NO ₂ → NO ₃

Notes: “OH + NO_2 ” represents oxidation reaction of OH radical and NO_2 , “HET N_2O_5 ” represents N_2O_5 heterogeneous hydrolysis reaction, “ NO_3 + VOC” represents series reactions of NO_3 radical with VOCs, “Others” represents the other production reactions of HNO_3 in CMAQ model, “ NO_2 + NO_3 ” represents reaction of NO_2 and NO_3 to form N_2O_5 and “ O_3 + NO_2 ” represents reaction of O_3 and NO_2 to form NO_3 radical. The species of “AMTNO3J” and “AISOPNNJ” are secondary organic aerosols (SOA) from monoterpene nitrates and isoprene dinitrates, respectively.

2.2. Observation Data

The meteorological surface observations, including 2 m temperature (T_2), 2 m relative humidity (RH_2), and 10 m wind speed (WS_{10}) with temporal resolution of 3 h at 10 stations (marked with red dots in Figure 1), were obtained from the website of <https://www.>

[ncei.noaa.gov/maps/hourly/](https://www.epa.gov/nci/noaa.gov/maps/hourly/) (last access: 10 May 2024). The data on hourly PM_{2.5} and O₃ concentration were downloaded from the China National Environmental Monitoring Center (CNEMC, <http://106.37.208.233:20035>, last access: 10 May 2024). According to the Chinese National Ambient Air Quality Standard (NAAQS), the concentrations of MDA8 O₃ (daily mean PM_{2.5}) exceed the Grade I and II air quality standards when concentrations are higher than 100 µg m⁻³ (35 µg m⁻³) and 160 µg m⁻³ (75 µg m⁻³), respectively. In this study, we define the combined O₃ and PM_{2.5} pollution process as a period of at least 5 consecutive days in which the MDA8 O₃ concentration exceeds 100 µg m⁻³ and daily mean PM_{2.5} concentration simultaneously over 35 µg m⁻³. Following this definition, we perform simulations of five co-pollution episodes of O₃ and PM_{2.5} in the NCP region: Episode 1 spans from 16 to 22 May 2017; Episode 2 from 11 to 2 June 2017; Episode 3 from 25 June to 7 July 2017; Episode 4 from 30 May to 8 June 2018; Episode 5 from 11 to 23 June 2018.

3. Results and Discussion

3.1. Model Evaluation

In this section, the performance of the model is validated using observed meteorological and chemical variables of the surface layer averaged over observation sites in the NCP region. Figure 2 shows the model simulation results compared with 3-hourly observed meteorological parameters. Overall, the WRF model performs well and can reproduce the variations in T₂, RH₂, and WS₁₀ during the air pollution episodes. The simulation results of T₂ and RH₂ exhibit a good agreement with observations; correlation coefficient (*R*) values range from 0.94 to 0.97 and 0.91 to 0.96, respectively. The *R* values of WS₁₀ (0.69 to 0.83) were lower in the different episodes than in T₂ and RH₂, with 38.47% to 53.76% overestimation compared to the meteorological observation. This tendency of overestimation in WS₁₀ has been widely reproduced in previous studies, which can be attributed to the unresolved topographic features in the surface drag parameterization and the coarse resolution [49,50].

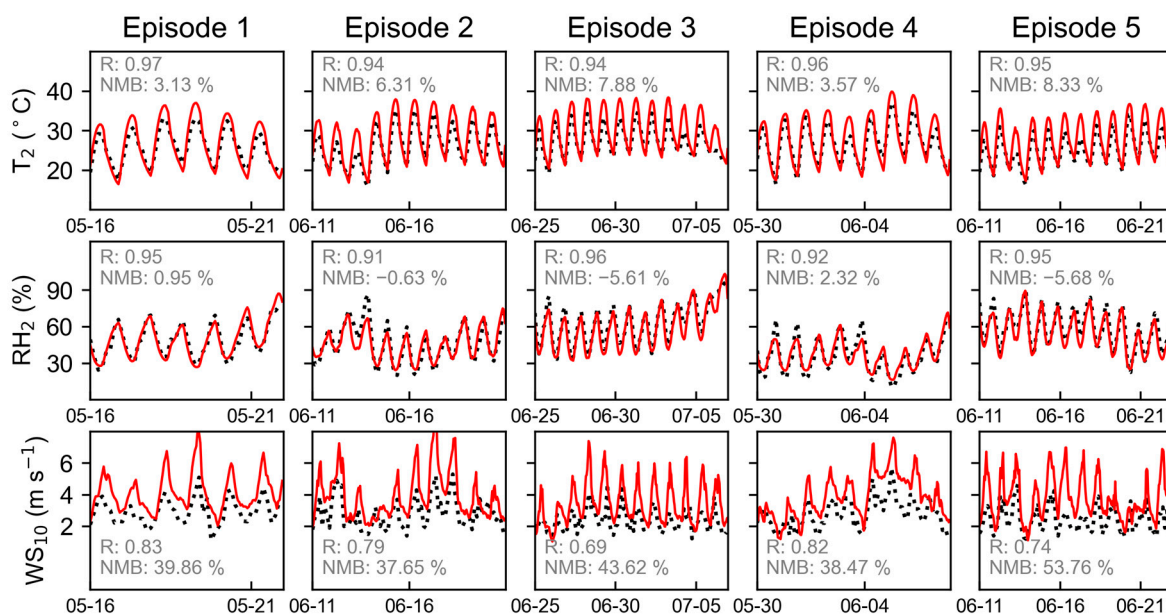


Figure 2. Time series of 3 hourly observations (black dashed line) and hourly simulation (red solid line), 2 m temperature (T₂), 2 m relative humidity (RH₂), and 10 m wind speed (WS₁₀) during the five air pollution episodes. The statistical metric correlation coefficient (*R*) and normalized mean bias (NMB) are shown.

Figure 3 shows the time series of observed and simulated major air pollutants over the NCP region for the five episodes. The simulated temporal variation of O₃ illustrates good agreement with the observed data, with *R* values of 0.88 to 0.93 for pollution episodes.

Compared to the hourly observed O_3 concentrations, the CMAQ model shows a slight underestimation, with the NMB of -3.08% to -37.66% . For $PM_{2.5}$, the R and NMB are 0.51 to 0.73 and -13.61% to -29.55% , respectively. The negative bias in $PM_{2.5}$ simulation results is attributed to the uncertainty of anthropogenic emissions and the deviation between the simulated meteorological field and reality [51–53]. Despite the underestimation of O_3 and $PM_{2.5}$, the simulated results reasonably reproduce the temporal and spatial variations of the pollution episodes.

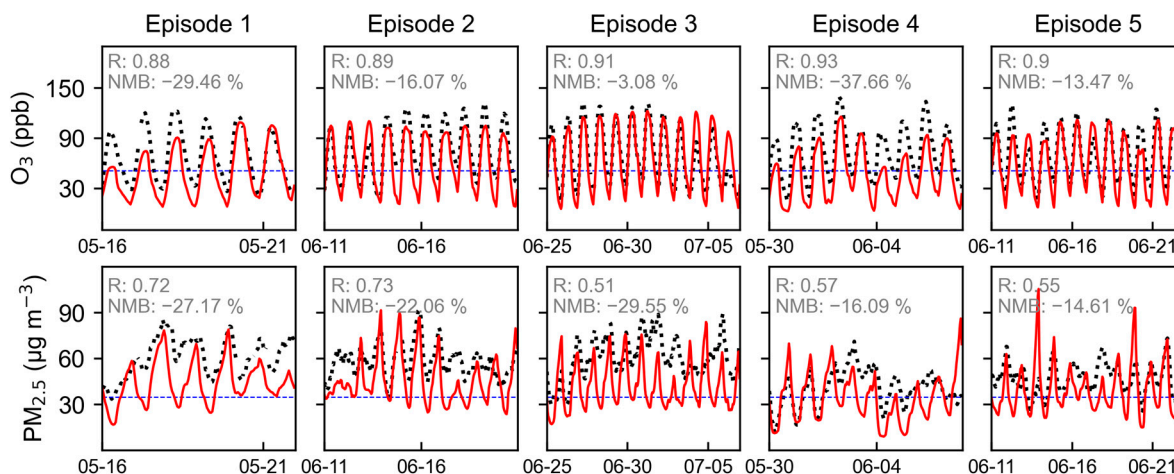


Figure 3. Time series of hourly observation (black dashed line) and simulation (red solid line) O_3 (ppb) and $PM_{2.5}$ ($\mu\text{g m}^{-3}$) concentration during the five air pollution episodes. The statistical metric correlation coefficient (R) and normalized mean bias (NMB) are shown. The values of $100 \mu\text{g m}^{-3}$ (51 ppb) and $35 \mu\text{g m}^{-3}$ were marked with blue dashed lines, respectively.

3.2. Diurnal Variation of $PM_{2.5}$ Components

Figure 4 illustrates the average hourly concentrations of $PM_{2.5}$ components and O_3 for five pollution episodes in the NCP region. The diurnal variations of O_3 and $PM_{2.5}$ are completely opposite, with O_3 concentrations peaking in the afternoon (15:00–17:00) and reaching their lowest levels at midnight (3:00), while $PM_{2.5}$ shows the opposite trend. The concentrations of NO_3^- and NH_4^+ in $PM_{2.5}$ exhibit similar temporal variations, with the lowest values being reached in the later afternoon (17:00) and elevating to the highest values before sunrise (5:00). Primary aerosols (including black carbon, dust and primary organic aerosol) also show similar variations, reaching a maximum concentration value in the early morning (5:00–6:00) and decline continued until the afternoon (16:00). Previous research has indicated that the uplift of planetary boundary layer height (PBLH) during the daytime creates favorable meteorological conditions for the diffusion of pollutants [54–56]. Meanwhile, the thermal decomposition of NO_3^- at high temperatures also inhibits its accumulation during the daytime [6]. In contrast to NO_3^- , NH_4^+ and primary aerosol diurnal cycle, SO_4^{2-} and secondary organic aerosol (SOA) do not show significant diurnal variations. SO_4^{2-} and SOA do not rapidly decrease as same as other $PM_{2.5}$ components (i.e., NO_3^- and NH_4^+) during daytime, suggesting that the concentrations of SO_4^{2-} and SOA are generated under strong atmospheric oxidation [57].

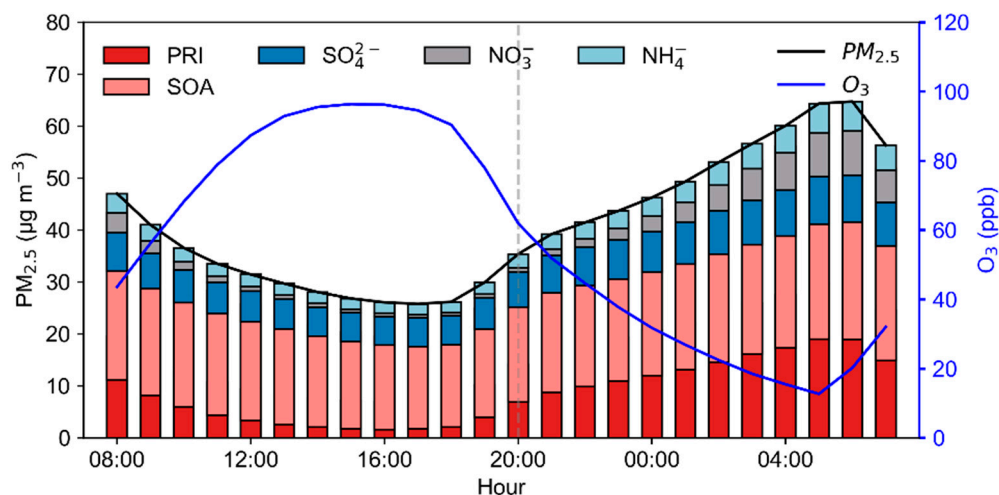


Figure 4. Average diurnal variations in concentrations of major $PM_{2.5}$ composition, O_3 , and $PM_{2.5}$ during pollution episodes. The black carbon (BC), dust, and primary organic aerosol (POA) are represented as primary aerosol components (PRI).

The average concentrations of NO_3^- , NH_4^+ , SO_4^{2-} and SOA are 2.9 , 3.3 , 7.0 , and $11.6 \mu\text{g m}^{-3}$ during the pollution episodes, accounting for 7.1%, 7.8%, 17.0% and 28.3% of $PM_{2.5}$ concentrations, respectively. Compared to daytime, nighttime $PM_{2.5}$ pollution is more severe, with concentrations increasing from 31.8 to $50.9 \mu\text{g m}^{-3}$. Concentrations of NO_3^- , NH_4^+ and primary $PM_{2.5}$ (PRI) increased significantly between 21:00 and 6:00, which account for 18%, 9%, and 65% of the increase in $PM_{2.5}$, respectively. Previous studies have indicated that favorable meteorological conditions (higher relative humidity, lower PBLH, and lower wind speed in the near-surface layer) are the basic environmental conditions for the uplift of $PM_{2.5}$ concentration [58–60]. However, the formation of secondary $PM_{2.5}$ components, especially secondary nitrate aerosols, also plays a significant role and cannot be neglected [61,62].

3.3. Nocturnal Formation Processes of Nitrate

The precursors (HNO_3 , N_2O_5 , and NO_x) and atmospheric oxidants (e.g., HO_x radicals, O_3 , and NO_3 radicals) are involved in the formation of NO_3^- [63,64]. The diurnal variation of the HNO_3 production rate generally presents a bimodal pattern, the first peak, 2.36 ppb h^{-1} , occurring at 12:00, and the second peak, 0.77 ppb h^{-1} , at midnight (22:00–23:00) (Figure 5a). The average production rate of HNO_3 is 1.7 ppb h^{-1} during daytime, which is slightly higher than the seasonal mean value of $1.55 \pm 0.59 \text{ ppb h}^{-1}$ in summer [46]. During the daytime (7:00 to 18:00), the “OH + NO_2 ” pathway dominates the production rate of HNO_3 , accounting for 97%. This is due to the strong photochemical effect during the daytime, which leads to the generation of a large number of hydroxyl (OH) radicals. Fu et al. and Liu et al. indicated that the reaction of NO_2 and OH is the predominant source of HNO_3 production, accounting for 89.9% in winter in the NCP region [32,65]. Consistent with our simulation results, Wen et al. indicated that the “OH + NO_2 ” pathway contributes between 94% and 96% to HNO_3 formation during the summer, which is slightly higher than the contribution in winter [6]. After the sunset (19:00 to 6:00), the contribution of the “OH + NO_2 ” pathway decreases to 40% for the total HNO_3 production rate. During the nighttime (19:00 to 6:00), the contribution of the “HET N_2O_5 ” and “ NO_3 + VOC” pathways increase to 57% and 3%, respectively. The formation of OH radicals essentially depend on the photolysis of VOCs and O_3 during daytime, while at night, the reaction between VOCs and O_3 replaces the photochemical reactions and becomes an important source of OH radicals [66,67]. As shown in Figure 5a, O_3 also maintains the formation of OH radicals immediately after sunset (20:00 to 21:00), thereby enhancing NO_3^- formation via

the “OH + NO₂” pathway, which accounts for 48% to 65% of total NO₃[−] production during this period.

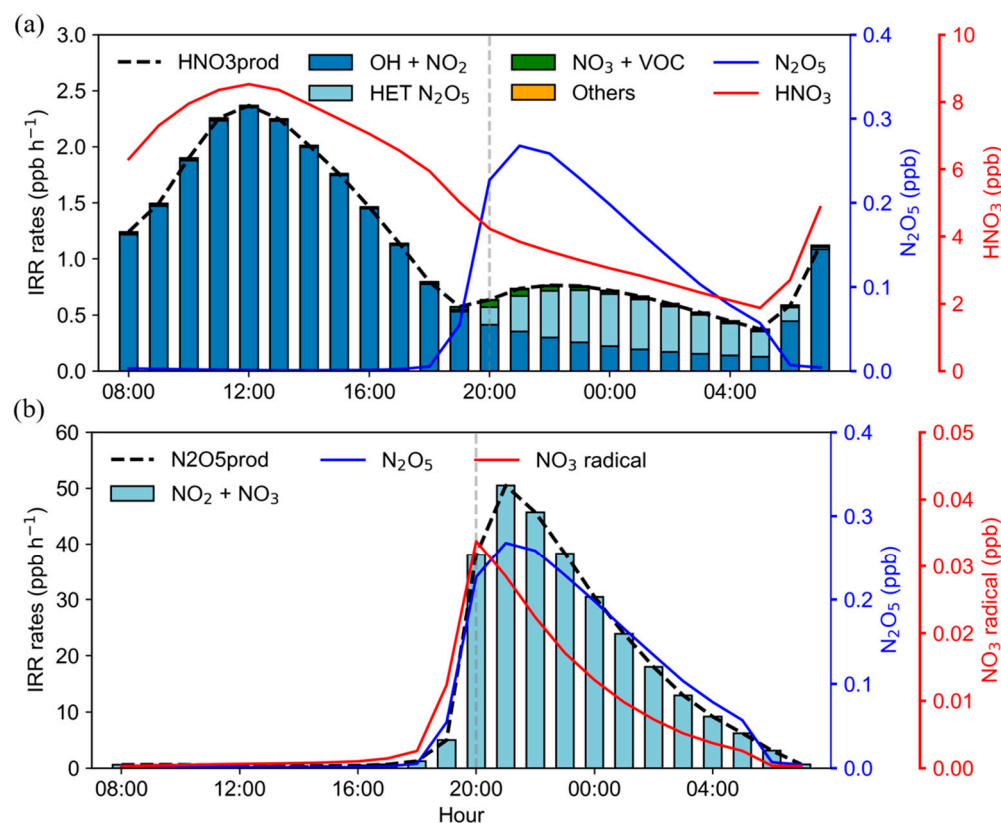


Figure 5. Average diurnal variations of (a) HNO₃ and (b) N₂O₅ production rates by different pathways, and associated with total HNO₃ production rates (HNO₃prod), total N₂O₅ production rates (N₂O₅prod), HNO₃, N₂O₅, and NO₃ radical concentrations during pollution episodes. “OH + NO₂”, “HET N₂O₅”, “NO₃ + VOC”, “Others” and “NO₂ + NO₃” represented different chemical reaction pathways described in Table 1 and Section 2.1.

The N₂O₅ heterogeneous hydrolysis reactions (“HET N₂O₅” pathway) are the dominant source of HNO₃, accounting for 60% to 67% of its production before sunrise (22:00 to 5:00). More favorable meteorological conditions at night facilitate the accumulation of NO₃[−]. Similarly, previous studies have simulated that the “HET N₂O₅” pathway is more important than “OH + NO₂” at nighttime, with a contribution of approximately 65% during summer and exhibiting a slightly higher contribution in winter, ranging from 83.6% to 97% [6,33,46,65]. Moreover, N₂O₅ is similar to HNO₃, and the uptake of N₂O₅ plays a key role in the NO₃ formation process. As shown in Figure 5b, the production rate of N₂O₅ increases at nighttime due to the reaction between NO₂ and NO₃ radicals. During the daytime, the NO₃ radical is rapidly photolyzed and reacts with NO, preventing its accumulation. The highest concentrations of N₂O₅ and NO₃ radicals occur after sunset (20:00 to 21:00). Observational studies have indicated that NO₃ radicals dominate the nocturnal gas-aerosol chemical reactions [68–71].

The NO₃ radical drives nocturnal NO₃[−] formation by reacting with NO₂ to produce N₂O₅. Previous studies have suggested that the reaction of O₃ and NO₂ is the essential source of the NO₃ radical compared to other chemical pathways [69,72]. As depicted in Figure 6, the concentration of NO₃ radical rises sharply after sunset (17:00), which coincides with a decrease in O₃ concentration. The diurnal variation of NO₃ production rate increases slightly after sunrise (5:00 to 10:00) and then decreases until 16:00, with two peaks occurring at 10:00 and 21:00. The simulation results illustrate that the NO₃ radical production rate exhibits a bimodal pattern attributed to the alter concentrations of O₃ and NO₂ during

the day. The production rate of NO_3 radical is restricted by the concentration of NO_2 and O_3 during daytime (8:00 to 19:00) and nighttime (20:00 to 7:00), respectively. Ma et al. indicated that reduced O_3 concentrations lead to decreased NO_3^- production (via N_2O_5 heterogeneous hydrolysis) in O_3 -limited areas [73]. Thus, O_3 plays a predominant role in the formation of NO_3 radicals at night, which subsequently drive the production of N_2O_5 and accelerate nocturnal NO_3^- formation.

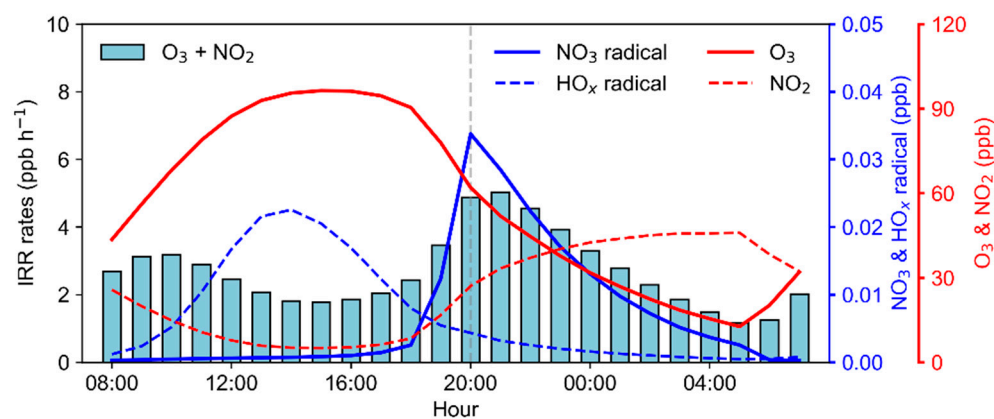


Figure 6. Average diurnal variations of NO_3 radical production rates from the “ $\text{O}_3 + \text{NO}_2$ ” pathway, the concentration of NO_3 radicals (blue solid line), HO_x radicals (blue dashed line), O_3 (red solid line) and NO_2 (red dashed line). “ $\text{O}_3 + \text{NO}_2$ ” represented chemical reaction pathway is described in Table 1 and Section 2.1.

4. Conclusions

In this study, we investigate the nocturnal NO_3^- formation processes during the co-pollution episodes of O_3 and $\text{PM}_{2.5}$ in the North China Plain (NCP) region using the WRF-CMAQ model. The simulation results indicate that the NO_3^- concentration increased by 3 times, contributing to an 18% increase in $\text{PM}_{2.5}$ concentration. The results of the IRR analysis illustrate that the reactions of OH radicals and NO_2 dominate HNO_3 production during daytime, accounting for 97%. However, unfavorable meteorological conditions during the daytime (high temperature and developed planetary boundary layer) constrained the accumulation of NO_3^- concentrations. Thus, NO_3^- concentrations frequently exhibit a rapid increase during the night. In the evening (20:00 to 21:00), the chemical reaction pathway of OH radicals and NO_2 accounts for 48% to 64% of NO_3^- formation, as the reaction between O_3 and VOCs sustains the formation of OH radicals even when photochemical reactions have ceased. During the midnight (22:00 to 5:00), N_2O_5 heterogeneous hydrolysis reaction is the predominant pathway for HNO_3 production, with an average accounting for 64%. The formation of N_2O_5 at night relies on the NO_3 radical, which is produced through the reaction between O_3 and NO_2 . Therefore, the rapid formation of O_3 during the daytime facilitates the formation of NO_3 radicals at night, thereby accelerating the nocturnal formation of NO_3^- in summer. Our results suggest that implementing a strategy to control O_3 pollution can also alleviate the rapid increase of NO_3^- at night.

There are some limitations in this work, such as the insufficient heterogeneous reaction processes at the surface of particulate matter in the model and uncertainties in NO_3^- precursors (e.g., NH_3 and NO_x) in anthropogenic emission inventory, which influence the model performance of NO_3^- . In addition, due to the lack of an effective method to diagnose the impact of O_3 on nocturnal atmospheric oxidation capacity, it is impossible to quantitatively estimate the contribution of O_3 and NO_x to nocturnal NO_3^- formation.

Author Contributions: Conceptualization, W.D. and M.X.; methodology, W.D.; software, W.D. and K.C.; validation, W.D., M.X. and X.H.; formal analysis, W.D.; investigation, W.D. and K.C.; resources, M.X.; data curation, M.X.; writing—original draft preparation, W.D.; writing—review and editing, W.D. and X.H.; visualization, W.D.; supervision, M.X.; project administration, M.X.; funding acquisition, M.X. All authors have read and agreed to the published version of the manuscript.

Funding: This work was supported by the National Natural Science Foundation of China (42177211).

Institutional Review Board Statement: Not applicable.

Informed Consent Statement: Not applicable.

Data Availability Statement: The data presented in this study are available on request from the corresponding author. The data are not publicly available due to the simulation data also forms part of an ongoing study.

Conflicts of Interest: The authors declare no conflict of interest.

References

1. Miller, L.; Xu, X. Ambient PM_{2.5} Human Health Effects—Findings in China and Research Directions. *Atmosphere* **2018**, *9*, 424. [[CrossRef](#)]
2. Wang, P.; Yang, Y.; Xue, D.; Ren, L.; Tang, J.; Leung, L.R.; Liao, H. Aerosols overtake greenhouse gases causing a warmer climate and more weather extremes toward carbon neutrality. *Nat. Commun.* **2023**, *14*, 7257. [[CrossRef](#)] [[PubMed](#)]
3. Li, K.; Jacob, D.J.; Shen, L.; Lu, X.; De Smedt, I.; Liao, H. Increases in surface ozone pollution in China from 2013 to 2019: Anthropogenic and meteorological influences. *Atmos. Chem. Phys.* **2020**, *20*, 11423–11433. [[CrossRef](#)]
4. Zhai, S.; Jacob, D.J.; Wang, X.; Liu, Z.; Wen, T.; Shah, V.; Li, K.; Moch, J.M.; Bates, K.H.; Song, S.; et al. Control of particulate nitrate air pollution in China. *Nat. Geosci.* **2021**, *14*, 389–395. [[CrossRef](#)]
5. Wang, J.; Gao, J.; Che, F.; Wang, Y.; Lin, P.; Zhang, Y. Decade-long trends in chemical component properties of PM_{2.5} in Beijing, China (2011–2020). *Sci. Total Environ.* **2022**, *832*, 154664. [[CrossRef](#)]
6. Wen, L.; Xue, L.; Wang, X.; Xu, C.; Chen, T.; Yang, L.; Wang, T.; Zhang, Q.; Wang, W. Summertime fine particulate nitrate pollution in the North China Plain: Increasing trends, formation mechanisms and implications for control policy. *Atmos. Chem. Phys.* **2018**, *18*, 11261–11275. [[CrossRef](#)]
7. Wang, Y.; Tang, G.; Zhao, W.; Yang, Y.; Wang, L.; Liu, Z.; Wen, T.; Cheng, M.; Wang, Y.; Wang, Y. Different roles of nitrate and sulfate in air pollution episodes in the North China Plain. *Atmos. Environ.* **2020**, *224*, 117325. [[CrossRef](#)]
8. Chen, X.; Wang, H.; Lu, K.; Li, C.; Zhai, T.; Tan, Z.; Ma, X.; Yang, X.; Liu, Y.; Chen, S.; et al. Field Determination of Nitrate Formation Pathway in Winter Beijing. *Environ. Sci. Technol.* **2020**, *54*, 9243–9253. [[CrossRef](#)]
9. Pan, Y.; Wang, Y.; Zhang, J.; Liu, Z.; Wang, L.; Tian, S.; Tang, G.; Gao, W.; Ji, D.; Song, T.; et al. Redefining the importance of nitrate during haze pollution to help optimize an emission control strategy. *Atmos. Environ.* **2016**, *141*, 197–202. [[CrossRef](#)]
10. Neuman, J.A.; Nowak, J.B.; Brock, C.A.; Trainer, M.; Fehsenfeld, F.C.; Holloway, J.S.; Hübler, G.; Hudson, P.K.; Murphy, D.M.; Nicks, D.K., Jr.; et al. Variability in ammonium nitrate formation and nitric acid depletion with altitude and location over California. *J. Geophys. Res. Atmos.* **2003**, *108*, 4557. [[CrossRef](#)]
11. Guo, H.; Sullivan, A.P.; Campuzano-Jost, P.; Schroder, J.C.; Lopez-Hilfiker, F.D.; Dibb, J.E.; Jimenez, J.L.; Thornton, J.A.; Brown, S.S.; Nenes, A.; et al. Fine particle pH and the partitioning of nitric acid during winter in the northeastern United States. *J. Geophys. Res. Atmos.* **2016**, *121*, 10355–10376. [[CrossRef](#)]
12. Morino, Y.; Kondo, Y.; Takegawa, N.; Miyazaki, Y.; Kita, K.; Komazaki, Y.; Fukuda, M.; Miyakawa, T.; Moteki, N.; Worsnop, D.R. Partitioning of HNO₃ and particulate nitrate over Tokyo: Effect of vertical mixing. *J. Geophys. Res. Atmos.* **2006**, *111*, D15215. [[CrossRef](#)]
13. Wang, Y.-L.; Song, W.; Yang, W.; Sun, X.-C.; Tong, Y.-D.; Wang, X.-M.; Liu, C.-Q.; Bai, Z.-P.; Liu, X.-Y. Influences of Atmospheric Pollution on the Contributions of Major Oxidation Pathways to PM_{2.5} Nitrate Formation in Beijing. *J. Geophys. Res. Atmos.* **2019**, *124*, 4174–4185. [[CrossRef](#)]
14. Vereecken, L.; Carlsson, P.T.M.; Novelli, A.; Bernard, F.; Brown, S.S.; Cho, C.; Crowley, J.N.; Fuchs, H.; Mellouki, W.; Reimer, D.; et al. Theoretical and experimental study of peroxy and alkoxy radicals in the NO₃-initiated oxidation of isoprene. *Phys. Chem. Chem. Phys.* **2021**, *23*, 5496–5515. [[CrossRef](#)]
15. Ren, Y.; McGillen, M.; Ouchen, I.; Daële, V.; Mellouki, A. Kinetic and product studies of the reactions of NO₃ with a series of unsaturated organic compounds. *J. Environ. Sci.* **2020**, *95*, 111–120. [[CrossRef](#)]
16. Wang, H.; Lu, K.; Chen, X.; Zhu, Q.; Chen, Q.; Guo, S.; Jiang, M.; Li, X.; Shang, D.; Tan, Z.; et al. High N₂O₅ Concentrations Observed in Urban Beijing: Implications of a Large Nitrate Formation Pathway. *Environ. Sci. Technol. Lett.* **2017**, *4*, 416–420. [[CrossRef](#)]
17. He, P.; Xie, Z.; Yu, X.; Wang, L.; Kang, H.; Yue, F. The observation of isotopic compositions of atmospheric nitrate in Shanghai China and its implication for reactive nitrogen chemistry. *Sci. Total Environ.* **2020**, *714*, 136727. [[CrossRef](#)]

18. Fan, M.-Y.; Zhang, Y.-L.; Lin, Y.-C.; Cao, F.; Zhao, Z.-Y.; Sun, Y.; Qiu, Y.; Fu, P.; Wang, Y. Changes of Emission Sources to Nitrate Aerosols in Beijing after the Clean Air Actions: Evidence from Dual Isotope Compositions. *J. Geophys. Res. Atmos.* **2020**, *125*, e2019JD031998. [[CrossRef](#)]
19. Zhou, W.; Zhao, J.; Ouyang, B.; Mehra, A.; Xu, W.; Wang, Y.; Bannan, T.J.; Worrall, S.D.; Priestley, M.; Bacak, A.; et al. Production of N₂O₅ and ClNO₂ in summer in urban Beijing, China. *Atmos. Chem. Phys.* **2018**, *18*, 11581–11597. [[CrossRef](#)]
20. Geyer, A.; Aliche, B.; Konrad, S.; Schmitz, T.; Stutz, J.; Platt, U. Chemistry and oxidation capacity of the nitrate radical in the continental boundary layer near Berlin. *J. Geophys. Res. Atmos.* **2001**, *106*, 8013–8025. [[CrossRef](#)]
21. Pathak, R.K.; Wang, T.; Wu, W.S. Nighttime enhancement of PM_{2.5} nitrate in ammonia-poor atmospheric conditions in Beijing and Shanghai: Plausible contributions of heterogeneous hydrolysis of N₂O₅ and HNO₃ partitioning. *Atmos. Environ.* **2011**, *45*, 1183–1191. [[CrossRef](#)]
22. Stark, H.; Lerner, B.M.; Schmitt, R.; Jakoubek, R.; Williams, E.J.; Ryerson, T.B.; Sueper, D.T.; Parrish, D.D.; Fehsenfeld, F.C. Atmospheric in situ measurement of nitrate radical (NO₃) and other photolysis rates using spectroradiometry and filter radiometry. *J. Geophys. Res. Atmos.* **2007**, *112*, D10S04. [[CrossRef](#)]
23. Yan, Y.; Wang, S.; Zhu, J.; Guo, Y.; Tang, G.; Liu, B.; An, X.; Wang, Y.; Zhou, B. Vertically increased NO₃ radical in the nocturnal boundary layer. *Sci. Total Environ.* **2021**, *763*, 142969. [[CrossRef](#)] [[PubMed](#)]
24. Stone, D.; Evans, M.J.; Walker, H.; Ingham, T.; Vaughan, S.; Ouyang, B.; Kennedy, O.J.; McLeod, M.W.; Jones, R.L.; Hopkins, J.; et al. Radical chemistry at night: Comparisons between observed and modelled HO_x, NO₃ and N₂O₅ during the RONOCO project. *Atmos. Chem. Phys.* **2014**, *14*, 1299–1321. [[CrossRef](#)]
25. Wang, H.; Wang, H.; Lu, X.; Lu, K.; Zhang, L.; Tham, Y.J.; Shi, Z.; Aikin, K.; Fan, S.; Brown, S.S.; et al. Increased night-time oxidation over China despite widespread decrease across the globe. *Nat. Geosci.* **2023**, *16*, 217–223. [[CrossRef](#)]
26. Ng, N.L.; Brown, S.S.; Archibald, A.T.; Atlas, E.; Cohen, R.C.; Crowley, J.N.; Day, D.A.; Donahue, N.M.; Fry, J.L.; Fuchs, H.; et al. Nitrate radicals and biogenic volatile organic compounds: Oxidation, mechanisms, and organic aerosol. *Atmos. Chem. Phys.* **2017**, *17*, 2103–2162. [[CrossRef](#)]
27. Juráň, S.; Grace, J.; Urban, O. Temporal Changes in Ozone Concentrations and Their Impact on Vegetation. *Atmosphere* **2021**, *12*, 82. [[CrossRef](#)]
28. Li, K.; Jacob, D.J.; Liao, H.; Qiu, Y.; Shen, L.; Zhai, S.; Bates, K.H.; Sulprizio, M.P.; Song, S.; Lu, X.; et al. Ozone pollution in the North China Plain spreading into the late-winter haze season. *Proc. Natl. Acad. Sci. USA* **2021**, *118*, e2015797118. [[CrossRef](#)]
29. Dai, H.; Liao, H.; Li, K.; Yue, X.; Yang, Y.; Zhu, J.; Jin, J.; Li, B.; Jiang, X. Composited analyses of the chemical and physical characteristics of co-polluted days by ozone and PM_{2.5} over 2013–2020 in the Beijing–Tianjin–Hebei region. *Atmos. Chem. Phys.* **2023**, *23*, 23–39. [[CrossRef](#)]
30. Li, M.; Wang, L.; Liu, J.; Gao, W.; Song, T.; Sun, Y.; Li, L.; Li, X.; Wang, Y.; Liu, L.; et al. Exploring the regional pollution characteristics and meteorological formation mechanism of PM_{2.5} in North China during 2013–2017. *Environ. Int.* **2020**, *134*, 105283. [[CrossRef](#)]
31. Wang, X.; Dickinson, R.E.; Su, L.; Zhou, C.; Wang, K. PM_{2.5} Pollution in China and How It Has Been Exacerbated by Terrain and Meteorological Conditions. *Bull. Am. Meteorol. Soc.* **2018**, *99*, 105–119. [[CrossRef](#)]
32. Fu, X.; Wang, T.; Gao, J.; Wang, P.; Liu, Y.; Wang, S.; Zhao, B.; Xue, L. Persistent Heavy Winter Nitrate Pollution Driven by Increased Photochemical Oxidants in Northern China. *Environ. Sci. Technol.* **2020**, *54*, 3881–3889. [[CrossRef](#)] [[PubMed](#)]
33. Lin, Y.C.; Zhang, Y.L.; Fan, M.Y.; Bao, M. Heterogeneous formation of particulate nitrate under ammonium-rich regimes during the high-PM_{2.5} events in Nanjing, China. *Atmos. Chem. Phys.* **2020**, *20*, 3999–4011. [[CrossRef](#)]
34. Wang, D.; Zhou, B.; Fu, Q.; Zhao, Q.; Zhang, Q.; Chen, J.; Yang, X.; Duan, Y.; Li, J. Intense secondary aerosol formation due to strong atmospheric photochemical reactions in summer: Observations at a rural site in eastern Yangtze River Delta of China. *Sci. Total Environ.* **2016**, *571*, 1454–1466. [[CrossRef](#)] [[PubMed](#)]
35. Wang, L.; Zhao, Y.; Liu, X.; Shi, J. Enhancement of atmospheric oxidation capacity induced co-pollution of the O₃ and PM_{2.5} in Lanzhou, northwest China. *Environ. Pollut.* **2024**, *341*, 122951. [[CrossRef](#)]
36. Wang, L.; Zhao, B.; Zhang, Y.; Hu, H. Correlation between surface PM_{2.5} and O₃ in eastern China during 2015–2019: Spatiotemporal variations and meteorological impacts. *Atmos. Environ.* **2023**, *294*, 119520. [[CrossRef](#)]
37. Wang, J.; Gao, J.; Che, F.; Yang, X.; Yang, Y.; Liu, L.; Xiang, Y.; Li, H. Summertime response of ozone and fine particulate matter to mixing layer meteorology over the North China Plain. *Atmos. Chem. Phys.* **2023**, *23*, 14715–14733. [[CrossRef](#)]
38. Appel, K.W.; Bash, J.O.; Fahey, K.M.; Foley, K.M.; Gilliam, R.C.; Hogrefe, C.; Hutzell, W.T.; Kang, D.; Mathur, R.; Murphy, B.N.; et al. The Community Multiscale Air Quality (CMAQ) model versions 5.3 and 5.3.1: System updates and evaluation. *Geosci. Model Dev.* **2021**, *14*, 2867–2897. [[CrossRef](#)]
39. Pye, H.O.T.; Murphy, B.N.; Xu, L.; Ng, N.L.; Carlton, A.G.; Guo, H.; Weber, R.; Vasilakos, P.; Appel, K.W.; Budisulistiorini, S.H.; et al. On the implications of aerosol liquid water and phase separation for organic aerosol mass. *Atmos. Chem. Phys.* **2017**, *17*, 343–369. [[CrossRef](#)]
40. Hersbach, H.; Bell, B.; Berrisford, P.; Hirahara, S.; Horányi, A.; Muñoz-Sabater, J.; Nicolas, J.; Peubey, C.; Radu, R.; Schepers, D.; et al. The ERA5 global reanalysis. *Q. J. R. Meteorol. Soc.* **2020**, *146*, 1999–2049. [[CrossRef](#)]
41. Chen, L.; Liao, H.; Li, K.; Zhu, J.; Long, Z.; Yue, X.; Yang, Y.; Zhang, M. Process-Level Quantification on Opposite PM_{2.5} Changes during the COVID-19 Lockdown over the North China Plain. *Environ. Sci. Technol. Lett.* **2023**, *10*, 779–785. [[CrossRef](#)]

42. Zheng, B.; Tong, D.; Li, M.; Liu, F.; Hong, C.; Geng, G.; Li, H.; Li, X.; Peng, L.; Qi, J.; et al. Trends in China's anthropogenic emissions since 2010 as the consequence of clean air actions. *Atmos. Chem. Phys.* **2018**, *18*, 14095–14111. [[CrossRef](#)]
43. Guenther, A.; Karl, T.; Harley, P.; Wiedinmyer, C.; Palmer, P.I.; Geron, C. Estimates of global terrestrial isoprene emissions using MEGAN (Model of Emissions of Gases and Aerosols from Nature). *Atmos. Chem. Phys.* **2006**, *6*, 3181–3210. [[CrossRef](#)]
44. Randerson, J.T.; Chen, Y.; van der Werf, G.R.; Rogers, B.M.; Morton, D.C. Global burned area and biomass burning emissions from small fires. *J. Geophys. Res. Biogeosci.* **2012**, *117*, G04012. [[CrossRef](#)]
45. Luecken, D.J.; Yarwood, G.; Hutzell, W.T. Multipollutant modeling of ozone, reactive nitrogen and HAPs across the continental US with CMAQ-CB6. *Atmos. Environ.* **2019**, *201*, 62–72. [[CrossRef](#)]
46. Sun, J.; Qin, M.; Xie, X.; Fu, W.; Qin, Y.; Sheng, L.; Li, L.; Li, J.; Sulaymon, I.D.; Jiang, L.; et al. Seasonal modeling analysis of nitrate formation pathways in Yangtze River Delta region, China. *Atmos. Chem. Phys.* **2022**, *22*, 12629–12646. [[CrossRef](#)]
47. Qu, K.; Wang, X.; Xiao, T.; Shen, J.; Lin, T.; Chen, D.; He, L.-Y.; Huang, X.-F.; Zeng, L.; Lu, K.; et al. Cross-regional transport of PM_{2.5} nitrate in the Pearl River Delta, China: Contributions and mechanisms. *Sci. Total Environ.* **2021**, *753*, 142439. [[CrossRef](#)]
48. Lin, Y.-C.; Cheng, M.-T.; Ting, W.-Y.; Yeh, C.-R. Characteristics of gaseous HNO₂, HNO₃, NH₃ and particulate ammonium nitrate in an urban city of Central Taiwan. *Atmos. Environ.* **2006**, *40*, 4725–4733. [[CrossRef](#)]
49. Tao, Z.; Chin, M.; Gao, M.; Kucsera, T.; Kim, D.; Bian, H.; Kurokawa, J.; Wang, Y.; Liu, Z.; Carmichael, G.R.; et al. Evaluation of NU-WRF model performance on air quality simulation under various model resolutions—An investigation within the framework of MICS-Asia Phase III. *Atmos. Chem. Phys.* **2020**, *20*, 2319–2339. [[CrossRef](#)]
50. Yu, E.; Bai, R.; Chen, X.; Shao, L. Impact of physical parameterizations on wind simulation with WRF V3.9.1.1 under stable conditions at planetary boundary layer gray-zone resolution: A case study over the coastal regions of North China. *Geosci. Model Dev.* **2022**, *15*, 8111–8134. [[CrossRef](#)]
51. Emery, C.; Liu, Z.; Russell, A.G.; Odman, M.T.; Yarwood, G.; Kumar, N. Recommendations on statistics and benchmarks to assess photochemical model performance. *J. Air Waste Manag. Assoc.* **2017**, *67*, 582–598. [[CrossRef](#)] [[PubMed](#)]
52. An, J.; Huang, Y.; Huang, C.; Wang, X.; Yan, R.; Wang, Q.; Wang, H.; Jing, S.; Zhang, Y.; Liu, Y.; et al. Emission inventory of air pollutants and chemical speciation for specific anthropogenic sources based on local measurements in the Yangtze River Delta region, China. *Atmos. Chem. Phys.* **2021**, *21*, 2003–2025. [[CrossRef](#)]
53. She, Y.; Li, J.; Lyu, X.; Guo, H.; Qin, M.; Xie, X.; Gong, K.; Ye, F.; Mao, J.; Huang, L.; et al. Current status of model predictions of volatile organic compounds and impacts on surface ozone predictions during summer in China. *Atmos. Chem. Phys.* **2024**, *24*, 219–233. [[CrossRef](#)]
54. Ma, S.; Shao, M.; Zhang, Y.; Dai, Q.; Xie, M. Sensitivity of PM_{2.5} and O₃ pollution episodes to meteorological factors over the North China Plain. *Sci. Total Environ.* **2021**, *792*, 148474. [[CrossRef](#)] [[PubMed](#)]
55. Liu, N.; Zhou, S.; Liu, C.; Guo, J. Synoptic circulation pattern and boundary layer structure associated with PM_{2.5} during wintertime haze pollution episodes in Shanghai. *Atmos. Res.* **2019**, *228*, 186–195. [[CrossRef](#)]
56. Shao, M.; Dai, Q.; Yu, Z.; Zhang, Y.; Xie, M.; Feng, Y. Responses in PM_{2.5} and its chemical components to typical unfavorable meteorological events in the suburban area of Tianjin, China. *Sci. Total Environ.* **2021**, *788*, 147814. [[CrossRef](#)]
57. Li, J.; Wang, G.; Zhang, Q.; Li, J.; Wu, C.; Jiang, W.; Zhu, T.; Zeng, L. Molecular characteristics and diurnal variations of organic aerosols at a rural site in the North China Plain with implications for the influence of regional biomass burning. *Atmos. Chem. Phys.* **2019**, *19*, 10481–10496. [[CrossRef](#)]
58. Chen, Z.; Chen, D.; Zhao, C.; Kwan, M.-p.; Cai, J.; Zhuang, Y.; Zhao, B.; Wang, X.; Chen, B.; Yang, J.; et al. Influence of meteorological conditions on PM_{2.5} concentrations across China: A review of methodology and mechanism. *Environ. Int.* **2020**, *139*, 105558. [[CrossRef](#)]
59. Dai, H.; Liao, H.; Wang, Y.; Qian, J. Co-occurrence of ozone and PM_{2.5} pollution in urban/non-urban areas in eastern China from 2013 to 2020: Roles of meteorology and anthropogenic emissions. *Sci. Total Environ.* **2024**, *924*, 171687. [[CrossRef](#)]
60. Sun, X.; Zhao, T.; Bai, Y.; Kong, S.; Zheng, H.; Hu, W.; Ma, X.; Xiong, J. Meteorology impact on PM_{2.5} change over a receptor region in the regional transport of air pollutants: Observational study of recent emission reductions in central China. *Atmos. Chem. Phys.* **2022**, *22*, 3579–3593. [[CrossRef](#)]
61. Guo, S.; Hu, M.; Zamora, M.L.; Peng, J.; Shang, D.; Zheng, J.; Du, Z.; Wu, Z.; Shao, M.; Zeng, L.; et al. Elucidating severe urban haze formation in China. *Proc. Natl. Acad. Sci. USA* **2014**, *111*, 17373–17378. [[CrossRef](#)] [[PubMed](#)]
62. Huang, R.-J.; Zhang, Y.; Bozzetti, C.; Ho, K.-F.; Cao, J.-J.; Han, Y.; Daellenbach, K.R.; Slowik, J.G.; Platt, S.M.; Canonaco, F.; et al. High secondary aerosol contribution to particulate pollution during haze events in China. *Nature* **2014**, *514*, 218–222. [[CrossRef](#)] [[PubMed](#)]
63. Womack, C.C.; McDuffie, E.E.; Edwards, P.M.; Bares, R.; de Gouw, J.A.; Docherty, K.S.; Dubé, W.P.; Fibiger, D.L.; Franchin, A.; Gilman, J.B.; et al. An Odd Oxygen Framework for Wintertime Ammonium Nitrate Aerosol Pollution in Urban Areas: NO_x and VOC Control as Mitigation Strategies. *Geophys. Res. Lett.* **2019**, *46*, 4971–4979. [[CrossRef](#)]
64. Tian, M.; Liu, Y.; Yang, F.; Zhang, L.; Peng, C.; Chen, Y.; Shi, G.; Wang, H.; Luo, B.; Jiang, C.; et al. Increasing importance of nitrate formation for heavy aerosol pollution in two megacities in Sichuan Basin, southwest China. *Environ. Pollut.* **2019**, *250*, 898–905. [[CrossRef](#)] [[PubMed](#)]
65. Liu, L.; Bei, N.; Hu, B.; Wu, J.; Liu, S.; Li, X.; Wang, R.; Liu, Z.; Shen, Z.; Li, G. Wintertime nitrate formation pathways in the north China plain: Importance of N₂O₅ heterogeneous hydrolysis. *Environ. Pollut.* **2020**, *266*, 115287. [[CrossRef](#)]

66. Zou, Z.; Chen, Q.; Xia, M.; Yuan, Q.; Chen, Y.; Wang, Y.; Xiong, E.; Wang, Z.; Wang, T. OH measurements in the coastal atmosphere of South China: Possible missing OH sinks in aged air masses. *Atmos. Chem. Phys.* **2023**, *23*, 7057–7074. [[CrossRef](#)]
67. Tan, Z.; Fuchs, H.; Lu, K.; Hofzumahaus, A.; Bohn, B.; Broch, S.; Dong, H.; Gomm, S.; Häsel, R.; He, L.; et al. Radical chemistry at a rural site (Wangdu) in the North China Plain: Observation and model calculations of OH, HO₂ and RO₂ radicals. *Atmos. Chem. Phys.* **2017**, *17*, 663–690. [[CrossRef](#)]
68. Wang, H.; Chen, X.; Lu, K.; Hu, R.; Li, Z.; Wang, H.; Ma, X.; Yang, X.; Chen, S.; Dong, H.; et al. NO₃ and N₂O₅ chemistry at a suburban site during the EXPLORE-YRD campaign in 2018. *Atmos. Environ.* **2020**, *224*, 117180. [[CrossRef](#)]
69. Wang, H.; Lu, K.; Chen, S.; Li, X.; Zeng, L.; Hu, M.; Zhang, Y. Characterizing nitrate radical budget trends in Beijing during 2013–2019. *Sci. Total Environ.* **2021**, *795*, 148869. [[CrossRef](#)]
70. Kiendler-Scharr, A.; Mensah, A.A.; Friese, E.; Topping, D.; Nemitz, E.; Prevot, A.S.H.; Äijälä, M.; Allan, J.; Canonaco, F.; Canagaratna, M.; et al. Ubiquity of organic nitrates from nighttime chemistry in the European submicron aerosol. *Geophys. Res. Lett.* **2016**, *43*, 7735–7744. [[CrossRef](#)]
71. Wang, Z.; Wang, W.; Tham, Y.J.; Li, Q.; Wang, H.; Wen, L.; Wang, X.; Wang, T. Fast heterogeneous N₂O₅ uptake and ClNO₂ production in power plant and industrial plumes observed in the nocturnal residual layer over the North China Plain. *Atmos. Chem. Phys.* **2017**, *17*, 12361–12378. [[CrossRef](#)]
72. Brown, S.S.; Stutz, J. Nighttime radical observations and chemistry. *Chem. Soc. Rev.* **2012**, *41*, 6405–6447. [[CrossRef](#)] [[PubMed](#)]
73. Ma, P.; Quan, J.; Dou, Y.; Pan, Y.; Liao, Z.; Cheng, Z.; Jia, X.; Wang, Q.; Zhan, J.; Ma, W.; et al. Regime-Dependence of Nocturnal Nitrate Formation via N₂O₅ Hydrolysis and Its Implication for Mitigating Nitrate Pollution. *Geophys. Res. Lett.* **2023**, *50*, e2023GL106183. [[CrossRef](#)]

Disclaimer/Publisher’s Note: The statements, opinions and data contained in all publications are solely those of the individual author(s) and contributor(s) and not of MDPI and/or the editor(s). MDPI and/or the editor(s) disclaim responsibility for any injury to people or property resulting from any ideas, methods, instructions or products referred to in the content.